Hindawi
Journal of Nanomaterials
Volume 2018, Article ID 1293847, 9 pages
https://doi.org/10.1155/2018/1293847

Research Article

UCNPs@$Zn_{0.5}Cd_{0.5}S$ Core-Shell and Yolk-Shell Nanostructures: Selective Synthesis, Characterization, and Near-Infrared-Mediated Photocatalytic Reduction of Cr(VI)

Wan-Ni Wang,[1] Wang Dong,[1] Chen-Xi Huang,[1] Bo Liu,[1] Sheng Cheng,[2] and Haisheng Qian[1,3]

[1]*School of Food and Bioengineering, Hefei University of Technology, Hefei 230009, China*
[2]*Instrumental Analysis Center, Hefei University of Technology, Hefei 230009, China*
[3]*Biomedical and Environmental Interdisciplinary Research Centre, Hefei 230010, China*

Correspondence should be addressed to Sheng Cheng; chengsh@hfut.edu.cn and Haisheng Qian; shqian@hfut.edu.cn

Received 29 May 2018; Accepted 9 August 2018; Published 13 September 2018

Academic Editor: Zhengping Zhou

Constructing near-infrared-light-mediated core-shell nanostructures incorporating upconversion nanoparticles (UCNPs) and semiconductors is of great importance for potential applications in photocatalysis, nano-biomedical engineering, solar cell, etc. In this work, we have demonstrated a two-step solution process to synthesize UCNPs@$Zn_{0.5}Cd_{0.5}S$ core-shell nanoparticles (CSN). Firstly, a layer of AA-Zn(Cd)$[OH]^{4-}$ composites was coated on UCNPs to form UCNPs@AA-Zn(Cd)$[OH]^{4-}$ composites, which has been converted to UCNPs@$Zn_{0.5}Cd_{0.5}S$ CSN via sulfidation reaction process using thioacetamide (TAA) as the sulfur source. Moreover, the UCNPs@$Zn_{0.5}Cd_{0.5}S$ yolk-shell nanoparticles (YSN) have been obtained from the UCNPs@$Zn_{0.5}Cd_{0.5}S$ CSN after calcination at 400°C, which show significantly photocatalytic activity for reduction of Cr(VI) under near-infrared light. All these can be attributed to the enhanced crystallization degree, resulting in enhanced energy transfer efficiency and separation efficiency of the photogenerated electrons and holes. An alternative strategy is provided in this study for fabrication of UCNP/semiconductor composites for various applications.

1. Introduction

The photocatalytic technology driven by solar light has become more and more attractive because solar energy is one of the most abundant resources [1–5]. Heterogeneous photocatalytic techniques based on semiconductor materials are widely used in photocatalytic decomposition of water, CO_2 reduction, and organic reactions [6–8]. Semiconductor materials have their unique electronic band structure, which will produce highly reactive electrons and holes when the electron of the valence band transits to the conduction band inspired by the light of appropriate wavelength. Moreover, the photogenerated electrons can reduce Cr(VI) under sunlight or simulated sunlight irradiation [9–12]. However, most of the semiconductor photocatalysts can only be activated with UV or visible light. In particular, near-infrared (NIR) light occupies more than 40% of the incoming solar energy, which makes it more significant to fabricate and develop photocatalysts driven by NIR light [13–16]. Despite this, the traditional plasmonic nanoparticles which can be absorbed in the NIR region are used in catalysis, bioimaging, and so on [17–19]. However, lanthanide ions doped upconversion nanoparticles (UCNPs), which can convert infrared energy to UV–Vis energy and excite semiconductors to broaden the scope of the spectral response and raise the utilization ratio of solar energy. Up to date, much effort has been devoted to fabricate NIR-light-mediated UCNP-based nanocomposites to fully utilize solar energy [20–26], including UCNPs@CuS [27–30], UCNPs@ZnO [31–33],

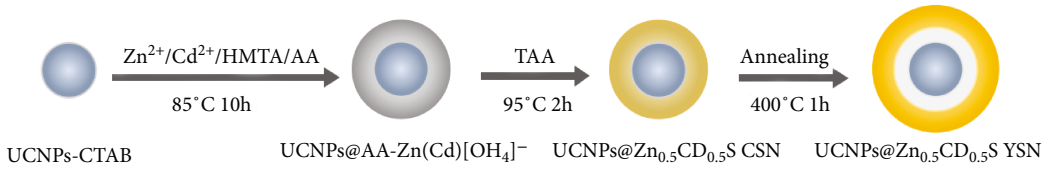

Figure 1: Schematic description of selective synthesis of UCNPs@$Zn_{0.5}Cd_{0.5}S$ core-shell and yolk-shell nanoparticles.

UCNPs@TiO_2 [34–37], UCNPs@Bi_2WO_6 [38, 39], and UCNPs@Bi_2MoO_6 [40–42]. As for the UCNP/semiconductor composites, the fluorescence energy can be passed from UCNPs (donors) to semiconductors (acceptors) to broaden the scope of the spectral response of the semiconductor effectively. These composite materials exhibit encouraging therapeutic efficacy of photodynamic therapy and the photochemical oxidation of organic matter under irradiation of NIR light [43, 44]. Many synthetic strategies including the epitaxial growth method, chemical assembly method, hydrothermal method, and electrospinning technique have been pioneered to fabricate UCNP-based Förster resonance energy transfer (FRET) nanostructures [45–49]. However, the large lattice mismatch makes it difficult for coating directly a layer of semiconductors on the surface of UCNPs.

Herein, a facile chemical solution process has been proposed to synthesize UCNPs@$Zn_{0.5}Cd_{0.5}S$ core-shell nanoparticles (CSN), in which UCNPs@AA-Zn(Cd)$[OH]^{4-}$ composites are firstly synthesized and subsequently converted to UCNPs@$Zn_{0.5}Cd_{0.5}S$ CSN by liquid sulfidation, as shown in Figure 1(a). UCNPs@$Zn_{0.5}Cd_{0.5}S$ yolk-shell nanoparticles (YSN) can be derived from the as-obtained core-shell nanoparticles of UCNPs@$Zn_{0.5}Cd_{0.5}S$ after calcination owing to the UCNPs@$Zn_{0.5}Cd_{0.5}S$ CSN incorporated by the surfactant. The optical properties of the samples have been studied carefully, and photochemical reduction tests of Cr(VI) ions are demonstrated.

2. Experimental

All the chemicals are of analytic grade and used as received. Hydrophilic $NaYF_4$:Yb(30%)/Tm(0.5%)@$NaYF_4$ (denoted as UCNPs) has been fabricated according to previously reported protocol [50, 51].

2.1. Synthesis of UCNPs@AA-Zn(Cd)$[OH]^{4-}$ Composites. In a typical process, 262.32 mg hexadecyltrimethylammonium bromide (CTAB) and 4.2 mg l-ascorbic acid (AA) were added into a 100 mL flask and dissolved using 60 mL deionized water to form clear solution. 2 mg as-prepared hydrophilic UCNPs, 25.24 mg hexamethylenetetramine (HMTA), 26.78 mg $Zn(NO_3)_2{\cdot}6H_2O$, and 18.66 mg $Cd(CH_3COO)_2{\cdot}2H_2O$ with an equal mole ratio of Zn/Cd were added into the previous solution with stirring. Subsequently, the mixed solution was heated to 85°C and maintained for 10 h. Finally, the solution was centrifuged after cooling to room temperature at a speed of 9500 rpm to collect the products, then washed with ethanol and deionized water for three times, and dried naturally. The yield of the UCNPs@AA-Zn(Cd)$[OH]^{4-}$ composites is about 90%.

2.2. Synthesis of UCNPs@$Zn_{0.5}Cd_{0.5}S$ Core-Shell and Yolk-Shell Nanoparticles. Typically, 20 mg previously prepared UCNPs@AA-Zn(Cd)$[OH]^{4-}$ composites and 3.76 mg TAA were added into a flask, which was dispersed using 15 mL deionized water and stirred for 12 h, then the temperature was raised to 95°C and kept for 2 h. The product in yellow was centrifugally separated (9500 rpm, 5 min) and the precipitate washed with deionized water and ethanol to remove the redundant ions. The as-synthesized UCNPs@$Zn_{0.5}Cd_{0.5}S$ core-shell nanoparticles were placed into a muffle furnace and then calcined at 400°C for 1 h to form UCNPs@$Zn_{0.5}Cd_{0.5}S$ yolk-shell nanoparticles (UCNPs@$Zn_{0.5}Cd_{0.5}S$ YSN). For comparison, UCNPs@ZnS CSN and UCNPs@ZnS YSN have been synthesized according to the same protocol. The yield of products at this stage is up to more than 95%.

2.3. Photocatalytic Activity. In a typical process, 5 mg of the photocatalyst was added under stirring into 50 mL of Cr(VI) solution (20 mg L^{-1}) which were prepared by dissolving $K_2Cr_2O_7$ into distilled water. The mixture was magnetically stirred for 1 h in the dark till adsorption-desorption equilibrium before irradiation. The solution was under irradiation of a 1500 mW cm^{-2} xenon lamp (PLX-300D, Beijing Precise Technology Co. Ltd.) with an emission wavelength of 320 nm–2500 nm. The NIR band (780–2500 nm) was obtained by equipping with an UV–Vis filter. The photocatalyst was centrifugally separated (9500 rpm, 2 min), and the Cr(VI) concentration was determined by diphenylcarbazide (DPC) method.

3. Results and Discussion

In this work, UCNPs with ca. 42 nm in diameter have been prepared and used as NIR light nanotransducers (Figure S1a, in the Supporting Information) [50]. The UCNPs@AA-Zn(Cd)$[OH]^{4-}$ core-shell composites with 20 nm in shell thickness were synthesized by a modified process [33], as revealed by TEM image shown in Figure S1b (in the Supporting Information). The FESEM and TEM images of the sample, which were obtained from UCNPs@AA-Zn(Cd)$[OH]^{4-}$ composites and thioacetamide (TAA) at 95°C for 2 h have been shown in Figures 2(a)–2(c), showing the sample consisted of core-shell nanoparticles. The elemental images shown in Figure S2 (in the Supporting Information) confirm the chemical composition of the as-obtained sample. It is interesting to note that the

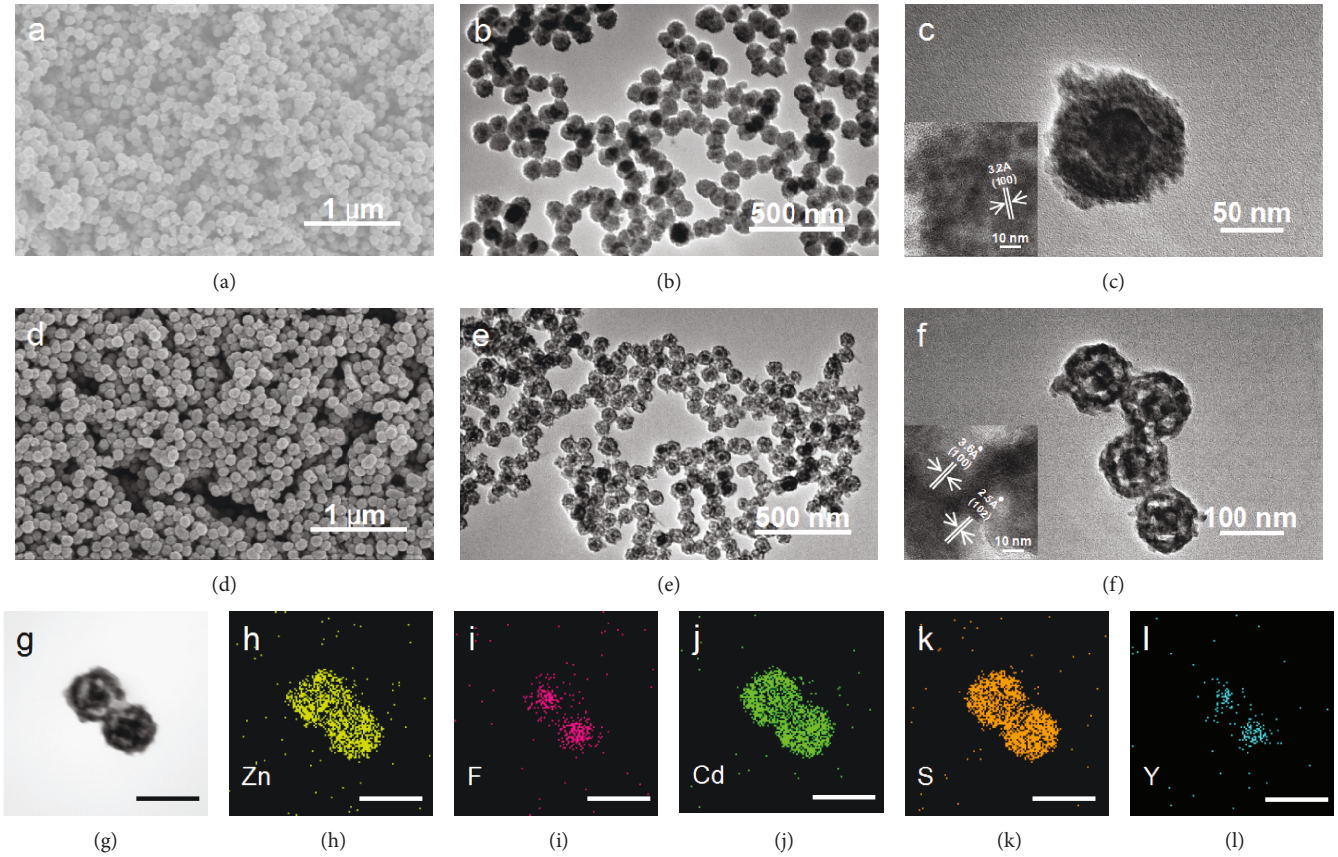

FIGURE 2: (a–c) FESEM, TEM, and HRTEM images of UCNPs@$Zn_{0.5}Cd_{0.5}S$ CSN. (d–f) FESEM, TEM, and HRTEM images of UCNPs@$Zn_{0.5}Cd_{0.5}S$ YSN. (g) STEM image of the UCNPs@$Zn_{0.5}Cd_{0.5}S$ YSN. (h–l) Elemental mapping images; the scale bars are 100 nm.

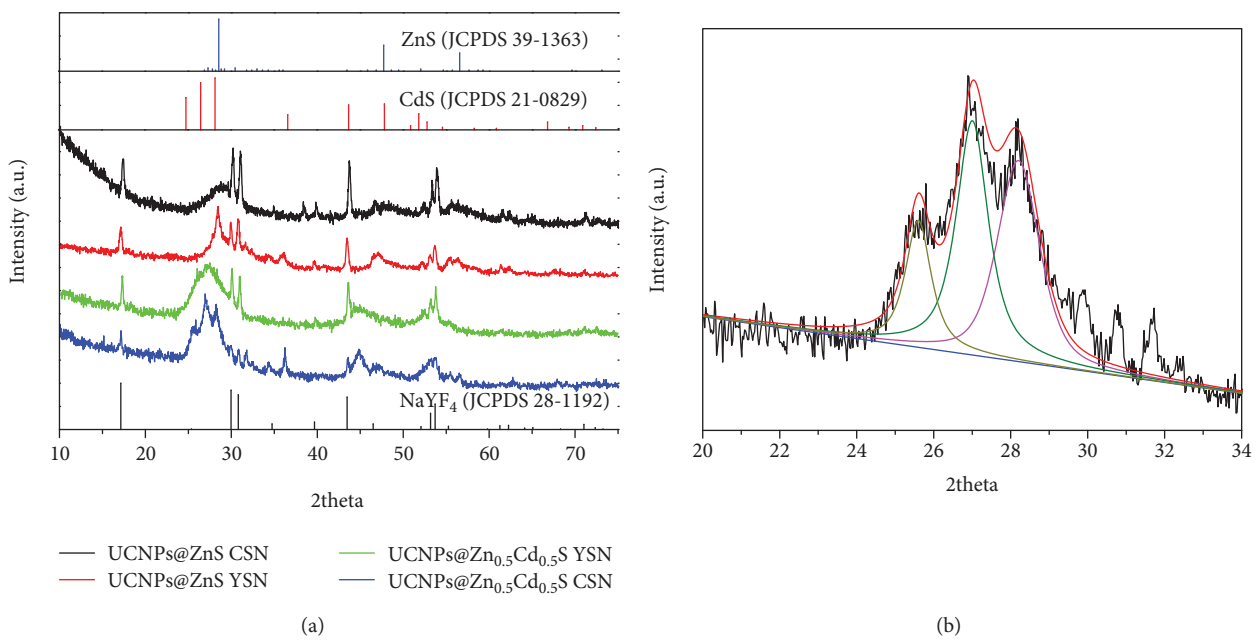

FIGURE 3: XRD patterns of the samples including UCNPs@ZnS CSN, UCNPs@ZnS YSN, UCNPs@$Zn_{0.5}Cd_{0.5}S$ CSN, and UCNPs@$Zn_{0.5}Cd_{0.5}S$ YSN.

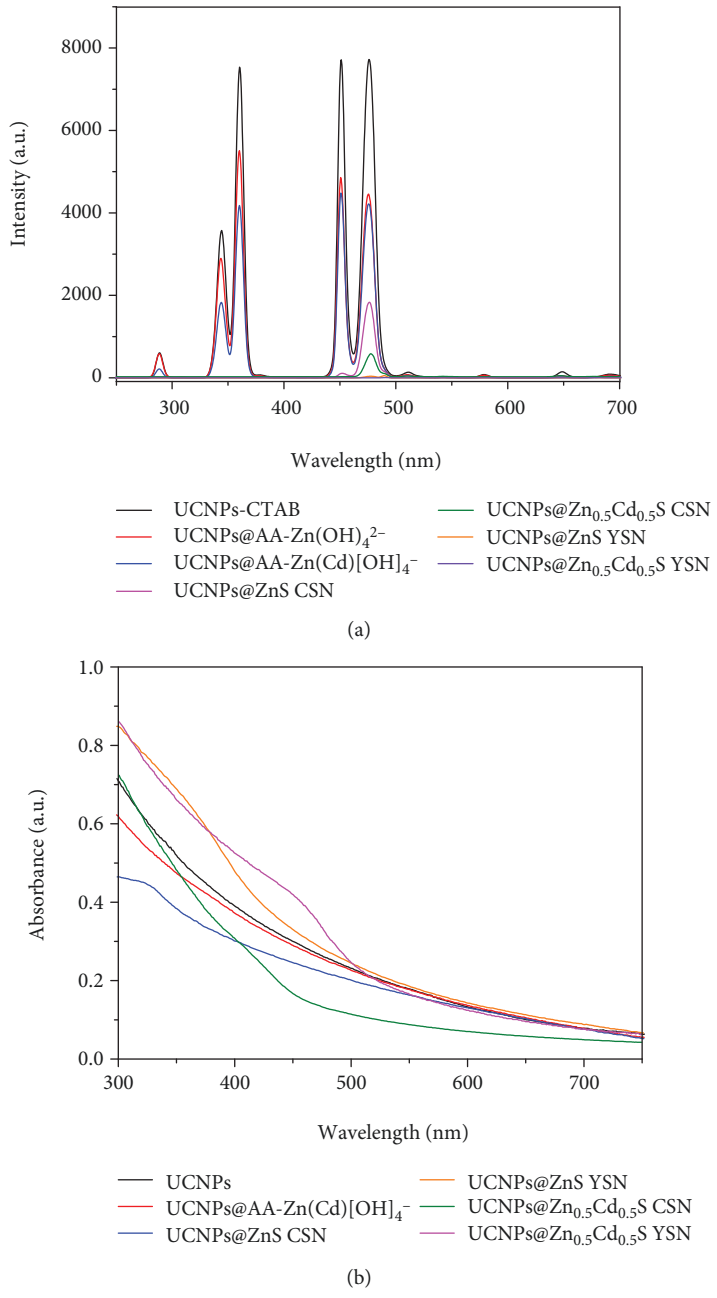

Figure 4: Fluorescence spectra (a) and UV–Vis absorbance (b) of different samples.

UCNPs@$Zn_xCd_{1-x}S$ CSN has been converted to the yolk-shell-like nanoparticles obtained after annealing at 400°C for 1 h and the yolk-shell nanoparticles are ca. 80 nm in total diameter and 20 nm in shell thickness (Figures 2(d) and 2(e)). The lattice spacing of 3.6 and 2.5 Å from the shell edge is shown in Figure 2(f), which is a little smaller than that of the (100) and (102) crystal plane of CdS nanostructures [43], confirming that the shell component is alloyed $Zn_xCd_{1-x}S$. The STEM and elemental mapping images including Zn, F, Cd, and Y are shown in Figures 2(g)–2(l), which further confirm that the yolk-shell nanoparticles with a shell consisted of elements of Zn, Cd, and S. X-ray diffraction (XRD) has been used to characterize the phase of the samples. All the sharper diffraction peaks (Figure 3(a)) coincide perfectly with the β-$NaYF_4$ (JCPDS no. 28–1192). On the side, the broad diffraction peak at 27° shown in Figure 3(b) can be derived to three peaks located at 25.6, 27.0, and 28.2° by Gaussian curve, which obviously shifted to higher diffraction angles of CdS (JCPDS no. 41–1049) compared to the pure CdS diffraction peaks at 24.8, 26.5, and 28.1° [52]. The EDX spectrum (Figure S3, in the Supporting Information) and XPS of UCNPs@$Zn_xCd_{1-x}S$ YSN (Figure S4, in the Supporting Information) are also operated to decide the chemical composition of UCNPs@$Zn_xCd_{1-x}S$ YSN. The accurate chemical composition of Zn/Cd in UCNPs@$Zn_xCd_{1-x}S$ is 0.51/0.49, which has been calculated using atomic absorption spectroscopy (AAS). Therefore, all the above analyses

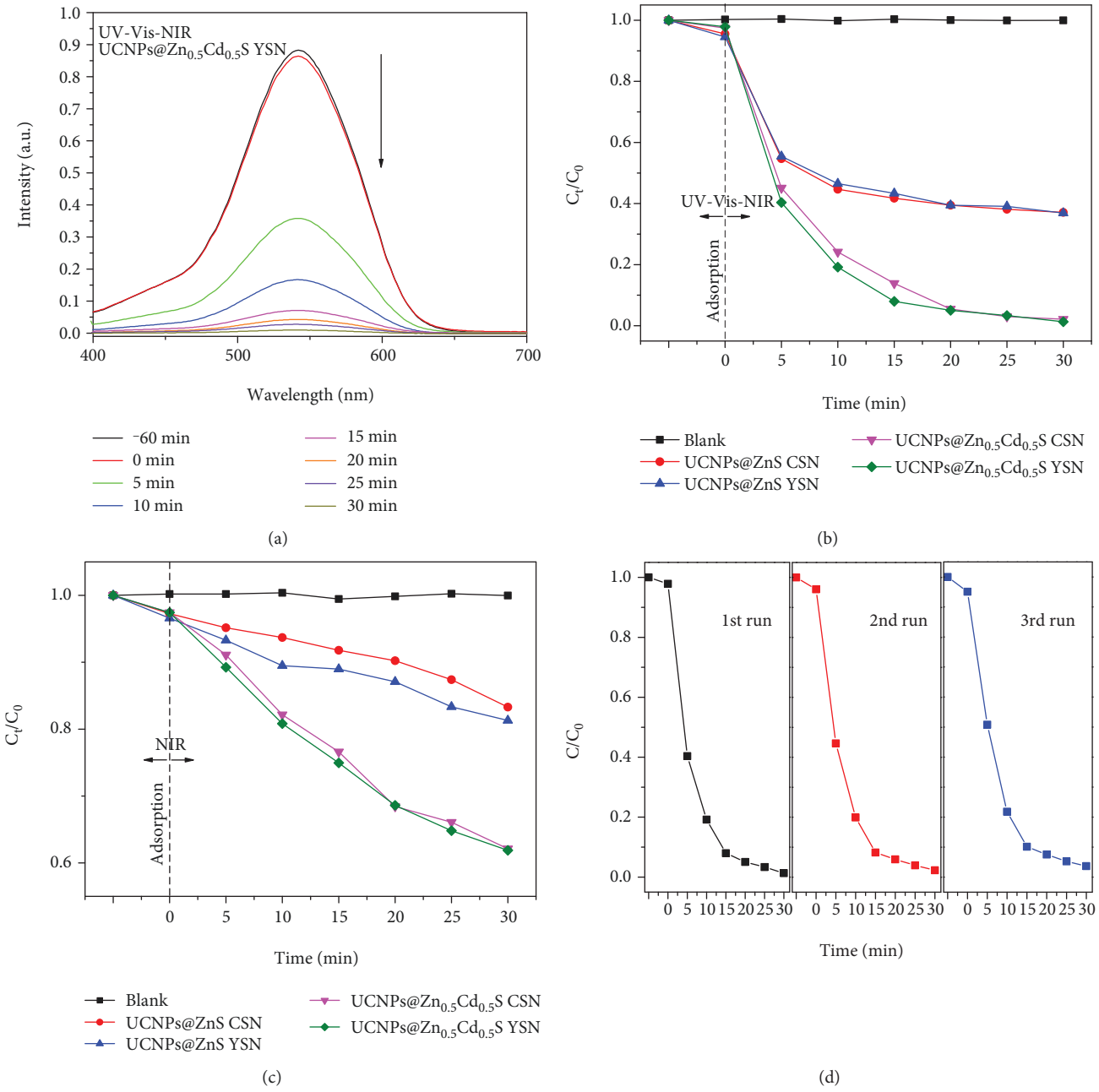

Figure 5: (a) UV–Vis spectra of the UV–Vis absorbance spectra of the Cr(VI) complex, showing the photochemical reduction ability of the UCNPs@$Zn_{0.5}Cd_{0.5}S$ YSN towards photocatalytic reduction of Cr(VI) at given irradiation times using a Xe lamp. (b, c) Photochemical reduction kinetic curves of Cr(VI) aqueous solution under irradiation of NIR light and a simulated solar light, respectively. C_0: the concentration of initial solution, C_t: the concentration at the irradiation time. (d) The three recycling tests of the photochemical reduction of Cr(VI) over the UCNPs@$Zn_{0.5}Cd_{0.5}S$ YSN.

demonstrate successive synthesis of the CSN and YSN of UCNPs@$Zn_{0.5}Cd_{0.5}S$. Herein, the UCNPs@$Zn_{0.5}Cd_{0.5}S$ CSN can be transferred to yolk-shell nanostructures because the shell ($Zn_{0.5}Cd_{0.5}S$) is comprised of lots of small nanoparticles stabilized by l-ascorbic acid (AA) molecules, as revealed by the FTIR spectra (Figure S5, in the Supporting Information). Some organic molecules or adsorbed functional group will be removed to form a void between the core and shell components during the annealing process whereas the small nanoparticles of $Zn_{0.5}Cd_{0.5}S$ would be aggregated and the crystallization degree of $Zn_{0.5}Cd_{0.5}S$ will be improved. As expected, the UCNPs@$Zn_{0.5}Cd_{0.5}S$ YSN show better photocatalytic ability than UCNPs@$Zn_{0.5}Cd_{0.5}S$ CSN.

The fluorescence spectra (Edinburgh FLS980, UK) and UV–visible spectra (Hitachi U-5100, Japan) have been used to study the optical properties of the samples. It is worthy to note that the fluorescence emissions at 342, 361, 451, and 476 nm (Figure 4(a)) for UCNPs@$Zn_{0.5}Cd_{0.5S}$ YSN have been quenched and the quenching efficiency is up to 99.90% for all the emissions (342, 361, 476, and 476 nm), confirming

that the yolk-shell nanoparticles show efficiently optical absorption and energy transfer between the yolk and shell. Figure 4(b) shows that the UCNPs@$Zn_{0.5}Cd_{0.5}S$ YSN exhibit stronger UV–Vis absorption at 400–600 nm, which overlap well with the fluorescence emissions of the UCNPs and will result in an efficient FRET process occurring between UCNPs and $Zn_{0.5}Cd_{0.5}S$. Thus, the as-prepared UCNPs@$Zn_{0.5}Cd_{0.5}S$ YSN will efficiently produce a large amount of reactive oxygen species including hydroxyl-free radicals ($^{\bullet}OH$) and photogenerated electrons under irradiation of NIR light or visible light.

In this work, the UCNPs can give ultraviolet–visible light emissions under excitation of NIR light, which can activate the shell component ($Zn_{0.5}Cd_{0.5}S$) via irradiation energy transfer (IET) or FRET process. The electron from the valence band of the excited shell can transit to the conduction band under the appropriate wavelength excitation, then a large amount of photogenerated electrons (e^-) is produced from the conduction band and positive hole (h^+) from the valence band [46, 53]. After that, the positive hole (h^+) can react with Cr(VI), which results in reduction of Cr(VI) to Cr(III). A rationalization mechanism for the photochemical reduction of Cr(VI) has been previously demonstrated as follows [54, 55]:

$$\begin{aligned} Zn_{0.5}Cd_{0.5}S + hv &\rightarrow h^+ + e^- \\ H_2O + h^+ &\rightarrow {}^{\bullet}OH + H^+ \\ Cr_2O_7^{2-} + 14H^+ + 6e^- &\rightarrow 2Cr^{3+} + 7H_2O \end{aligned} \quad (1)$$

The terephthalic acid (TA) was used to generate the fluorescent product for detecting $^{\bullet}OH$ radicals in solution [56, 57]. The fluorescence intensity of 2-hydroxy-terephthalic acid (TAOH) produced from terephthalic acid (TA) with $^{\bullet}OH$ shows a dramatic enhancement with time (Figure S6, in the Supporting Information) in the presence of UCNPs@$Zn_{0.5}Cd_{0.5}S$ YSN under irradiation of NIR light, which verified that the YSN has the great ability to produce $^{\bullet}OH$ and electrons. Thus, the as-prepared UCNPs@$Zn_{0.5}Cd_{0.5}S$ YSN would exhibit good NIR-mediated photochemical reduction or oxidation performance. In the present study, 50 mL (20 μg/mL) Cr(VI) aqueous solution was irradiated using infrared light (IR) or simulated solar light. Before irradiation, mixtures of the as-obtained photocatalysts and $K_2Cr_2O_7$ aqueous solution were stirred in the dark for 1 h to reach adsorption equilibrium. Diphenylcarbazide (DPC) method has been widely used to analyze the concentration of Cr(VI) [9]. As shown in Figure 5, there is no obvious change in the Cr(VI) concentration in the absence of the photocatalyst after irradiation for 1 h, whereas nearly 38.1% and 98.7% of Cr(VI) have been reduced to Cr(III) in 30 min for UCNPs@$Zn_{0.5}Cd_{0.5}S$ YSN under irradiation of a Xe lamp equipped with or without an UV–Vis filter. UCNPs@$Zn_{0.5}Cd_{0.5}S$ YSN has better photocatalytic activity property than UCNPs@$Zn_{0.5}Cd_{0.5}S$ CSN because of better crystallization during the annealing process and has the highest photocatalytic activity among all of the samples no matter with (Figure 5(b)) or without (Figure 5(c)) UV–Vis filter, indicating that the import of

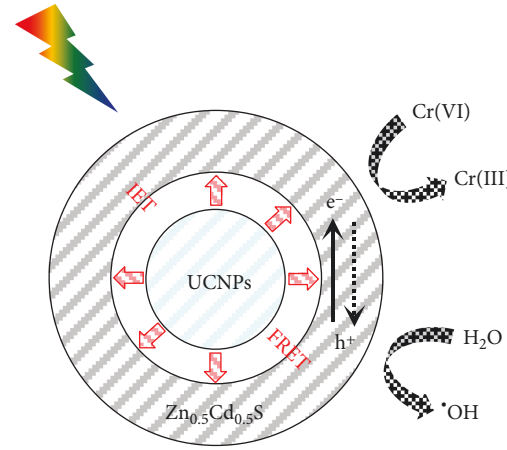

Scheme 1: Demonstration the NIR-light-mediated photochemical reduction process.

CdS can enhance the energy transfer efficiency between UCNPs with the shell. Additionally, in order to investigate the repeatability and chemical stability of photocatalyst, three uninterrupted cycling tests have been operated and shown in Figure 5(d). Therefore, the as-prepared UCNPs@$Zn_{0.5}Cd_{0.5}S$ YSN shows good chemical stability, which has a strong ability for producing $^{\bullet}OH$ and electrons for photochemical reduction of Cr(VI). The photocatalytic mechanism has been illustrated and summarized in Scheme 1. The synthetic method described here has demonstrated that it will provide an important strategy for constructing nanocomposite-incorporated UCNPs and semiconductors for NIR-mediated photochemical process.

4. Conclusions

In summary, we have synthesized UCNPs@$Zn_{0.5}Cd_{0.5}S$ core-shell and yolk-shell nanoparticles by a facile epitaxial growth process. UCNPs@AA-$[Zn_{0.5}Cd_{0.5}(OH)_4]^{2-}$ nanocomposites are firstly synthesized via a modified process, which can be converted to UCNPs@$Zn_{0.5}Cd_{0.5}S$ CSN via a sulfidation reaction. The UCNPs@$Zn_{0.5}Cd_{0.5}S$ YSN can be achieved after calcination of UCNPs@$Zn_{0.5}Cd_{0.5}S$ CSN at 400°C. In addition, the crystallization degree for the final UCNPs@$Zn_{0.5}Cd_{0.5}S$ YSN has been enhanced during the annealing process. The fluorescence emissions for Tm^{3+} in UCNPs@$Zn_{0.5}Cd_{0.5}S$ yolk-shell nanoparticles have been quenched greatly, demonstrating efficient energy transfer between the achieved two components of UCNPs and $Zn_{0.5}Cd_{0.5}S$. The as-obtained UCNPs@$Zn_{0.5}Cd_{0.5}S$ YSN exhibit superior photocatalytic activity for reduction of Cr(VI) under no matter simulated solar light or IR light. Therefore, this work should inspire further exploration for alterative nanoparticles with high potential for potential applications in nanomedicine, photocatalytic, energy conversion, etc.

Data Availability

The data used to support the findings of this study are available from the corresponding author upon request.

Conflicts of Interest

There are no conflicts of interest.

Authors' Contributions

W. Wang, F. Zhang, and W. Dong contributed equally to this work.

Acknowledgments

We acknowledge the funding supports from the National Natural Science Foundation of China (Grants 21471043 and 31501576).

Supplementary Materials

Figure S1: (a) transmission electron microscopy (TEM) image of $NaYF_4$:Yb/Tm@$NaYF_4$ nanoparticles. (b) Transmission electron microscopy (TEM) image of UCNPs@AA-Zn$[(OH)_4]^{2-}$ nanoparticles. Figure S2: STEM image and elemental imaging of UCNPs@$Zn_{0.5}Cd_{0.5}S$ CSN. Figure S3: (a) energy-dispersive X-ray spectra of the as-prepared product shown in Figure 1; (b) element composition of the as-prepared UCNPs@$Zn_{0.5}Cd_{0.5}S$ YSN from EDX analyses. Figure S4: X-ray photoelectron spectra of the as-prepared yolk-shell-like nanoparticles of UCNPs@$Zn_{0.5}Cd_{0.5}S$ YSN: (a) a general survey; (b) Zn 2p; (c) Cd 3d; (d) S 2p; (e) Na 1s; (f) Y 3d; (g) Yb 4d; and (h)Tm 4d. Figure S5: Fourier transform infrared (FT-IR) spectrum of the as-prepared UCNPs@$Zn_{0.5}Cd_{0.5}S$ CSN and UCNPs@$Zn_{0.5}Cd_{0.5}S$ YSN. Figure S6: (a) fluorescence spectra of 2-hydroxy-terephthalic acid (TAOH) with the addition of UCNPs@$Zn_{0.5}Cd_{0.5}S$ YSN excited by a 980 nm CW laser. (b) Photocatalytic reduction of Cr(VI) in the presence of UCNPs@$Zn_{0.5}Cd_{0.5}S$ YSN at given irradiation times under irradiation of a 1500 mW Xe lamp with a UV–Vis filter. *(Supplementary Materials)*

References

[1] H. Dong, G. Zeng, L. Tang et al., "An overview on limitations of TiO_2-based particles for photocatalytic degradation of organic pollutants and the corresponding countermeasures," *Water Research*, vol. 79, pp. 128–146, 2015.

[2] U. I. Gaya and A. H. Abdullah, "Heterogeneous photocatalytic degradation of organic contaminants over titanium dioxide: a review of fundamentals, progress and problems," *Journal of Photochemistry and Photobiology C: Photochemistry Reviews*, vol. 9, no. 1, pp. 1–12, 2008.

[3] N. Cheng, J. Tian, Q. Liu et al., "Au-nanoparticle-loaded graphitic carbon nitride nanosheets: green photocatalytic synthesis and application toward the degradation of organic pollutants," *ACS Applied Materials & Interfaces*, vol. 5, no. 15, pp. 6815–6819, 2013.

[4] X. Li, G. Chen, L. Yang, Z. Jin, and J. Liu, "Multifunctional Au-coated TiO_2 nanotube arrays as recyclable SERS substrates for multifold organic pollutants detection," *Advanced Functional Materials*, vol. 20, no. 17, pp. 2815–2824, 2010.

[5] Z. Li, S. Yang, J. Zhou et al., "Novel mesoporous g-C_3N_4 and $BiPO_4$ nanorods hybrid architectures and their enhanced visible-light-driven photocatalytic performances," *Chemical Engineering Journal*, vol. 241, pp. 344–351, 2014.

[6] M. N. Chong, B. Jin, C. W. K. Chow, and C. Saint, "Recent developments in photocatalytic water treatment technology: a review," *Water Research*, vol. 44, no. 10, pp. 2997–3027, 2010.

[7] M. Mehrjouei, S. Muller, and D. Moller, "A review on photocatalytic ozonation used for the treatment of water and wastewater," *Chemical Engineering Journal*, vol. 263, pp. 209–219, 2015.

[8] C. Yu, Z. Wu, R. Liu et al., "Novel fluorinated Bi_2MoO_6 nanocrystals for efficient photocatalytic removal of water organic pollutants under different light source illumination," *Applied Catalysis B: Environmental*, vol. 209, pp. 1–11, 2017.

[9] X. Gao, H. B. Wu, L. Zheng, Y. Zhong, Y. Hu, and X. W. D. Lou, "Formation of mesoporous heterostructured $BiVO_4/Bi_2S_3$ hollow discoids with enhanced photoactivity," *Angewandte Chemie International Edition*, vol. 53, no. 23, pp. 5917–5921, 2014.

[10] X. Meng, G. Zhang, and N. Li, "$Bi_{24}Ga_2O_{39}$ for visible light photocatalytic reduction of Cr(VI): controlled synthesis, facet-dependent activity and DFT study," *Chemical Engineering Journal*, vol. 314, pp. 249–256, 2017.

[11] L. Mao, J. Li, Y. Xie, Y. Zhong, and Y. Hu, "Controllable growth of SnS_2/SnO_2 heterostructured nanoplates via a hydrothermal-assisted self-hydrolysis process and their visible-light-driven photocatalytic reduction of Cr(vi)," *RSC Advances*, vol. 4, no. 56, pp. 29698–29701, 2014.

[12] G. M. Shi, B. Zhang, X. X. Xu, and Y. H. Fu, "Graphene oxide coated coordination polymer nanobelt composite material: a new type of visible light active and highly efficient photocatalyst for Cr(vi) reduction," *Dalton Transactions*, vol. 44, no. 24, pp. 11155–11164, 2015.

[13] Z.-F. Huang, J. Song, L. Pan, X. Zhang, L. Wang, and J.-J. Zou, "Tungsten oxides for photocatalysis, electrochemistry, and phototherapy," *Advanced Materials*, vol. 27, no. 36, pp. 5309–5327, 2015.

[14] S. Huang, S. Guo, Q. Wang et al., "CaF_2-based near-infrared photocatalyst using the multifunctional $CaTiO_3$ precursors as the calcium source," *ACS Applied Materials & Interfaces*, vol. 7, no. 36, pp. 20170–20178, 2015.

[15] D.-X. Xu, Z.-W. Lian, M.-L. Fu, B. Yuan, J.-W. Shi, and H.-J. Cui, "Advanced near-infrared-driven photocatalyst: fabrication, characterization, and photocatalytic performance of β-$NaYF_4$:Yb^{3+},Tm^{3+}@TiO_2 core@shell microcrystals," *Applied Catalysis B: Environmental*, vol. 142-143, pp. 377–386, 2013.

[16] X. Y. Kong, W. L. Tan, B. J. Ng, S. P. Chai, and A. R. Mohamed, "Harnessing Vis–NIR broad spectrum for photocatalytic CO_2 reduction over carbon quantum dots-decorated ultrathin Bi_2WO_6 nanosheets," *Nano Research*, vol. 10, no. 5, pp. 1720–1731, 2017.

[17] N. R. Jana, L. Gearheart, and C. J. Murphy, "Wet chemical synthesis of high aspect ratio cylindrical gold nanorods," *The Journal of Physical Chemistry B*, vol. 105, no. 19, pp. 4065–4067, 2001.

[18] A. U. Khan, Z. Zhou, J. Krause, and G. Liu, "Poly(vinylpyrrolidone)-free multistep synthesis of silver nanoplates with plasmon resonance in the near infrared range," *Small*, vol. 13, no. 43, 2017.

[19] V. Bastys, I. Pastoriza-Santos, B. Rodríguez-González, R. Vaisnoras, and L. M. Liz-Marzán, "Formation of silver nanoprisms with surface plasmons at communication wavelengths," *Advanced Functional Materials*, vol. 16, no. 6, pp. 766–773, 2006.

[20] J. Ni, C. Shan, B. Li et al., "Assembling of a functional cyclodextrin-decorated upconversion luminescence nanoplatform for cysteine-sensing," *Chemical Communications*, vol. 51, no. 74, pp. 14054–14056, 2015.

[21] X. Wu, Y. Zhang, K. Takle et al., "Dye-sensitized core/active shell upconversion nanoparticles for optogenetics and bioimaging applications," *ACS Nano*, vol. 10, no. 1, pp. 1060–1066, 2016.

[22] D. Lu, S. K. Cho, S. Ahn, L. Brun, C. J. Summers, and W. Park, "Plasmon enhancement mechanism for the upconversion processes in $NaYF_4$:Yb^{3+},Er^{3+} nanoparticles: Maxwell versus Förster," *ACS Nano*, vol. 8, no. 8, pp. 7780–7792, 2014.

[23] V. Muhr, C. Wurth, M. Kraft et al., "Particle-size-dependent Förster resonance energy transfer from upconversion nanoparticles to organic dyes," *Analytical Chemistry*, vol. 89, no. 9, pp. 4868–4874, 2017.

[24] G. Tian, W. Ren, L. Yan et al., "Red-emitting upconverting nanoparticles for photodynamic therapy in cancer cells under near-infrared excitation," *Small*, vol. 9, no. 11, pp. 1929–1938, 2013.

[25] L. Wang, R. Yan, Z. Huo et al., "Fluorescence resonant energy transfer biosensor based on upconversion-luminescent nanoparticles," *Angewandte Chemie International Edition*, vol. 44, no. 37, pp. 6054–6057, 2005.

[26] R. Lv, P. Yang, F. He et al., "A yolk-like multifunctional platform for multimodal imaging and synergistic therapy triggered by a single near-infrared light," *ACS Nano*, vol. 9, no. 2, pp. 1630–1647, 2015.

[27] R. Lv, P. Yang, B. Hu, J. Xu, W. Shang, and J. Tian, "In situ growth strategy to integrate up-conversion nanoparticles with ultrasmall CuS for photothermal theranostics," *ACS Nano*, vol. 11, no. 1, pp. 1064–1072, 2017.

[28] B. Liu, C. Li, Z. Xie et al., "808 nm photocontrolled UCL imaging guided chemo/photothermal synergistic therapy with single UCNPs-CuS@PAA nanocomposite," *Dalton Transactions*, vol. 45, no. 33, pp. 13061–13069, 2016.

[29] G. Yang, R. Lv, F. He et al., "A core/shell/satellite anticancer platform for 808 NIR light-driven multimodal imaging and combined chemo-/photothermal therapy," *Nanoscale*, vol. 7, no. 32, pp. 13747–13758, 2015.

[30] C. X. Huang, H. J. Chen, F. Li et al., "Controlled synthesis of upconverting nanoparticles/CuS yolk–shell nanoparticles for in vitro synergistic photothermal and photodynamic therapy of cancer cells," *Journal of Materials Chemistry B*, vol. 5, no. 48, pp. 9487–9496, 2017.

[31] S. Huang, H. Wang, N. Zhu et al., "Metal recovery based magnetite near-infrared photocatalyst with broadband spectrum utilization property," *Applied Catalysis B: Environmental*, vol. 181, pp. 456–464, 2016.

[32] W. N. Wang, F. Zhang, C. L. Zhang, Y. C. Guo, W. Dai, and H. S. Qian, "Fabrication of zinc oxide composite microfibers for near-infrared-light-mediated photocatalysis," *ChemCatChem*, vol. 9, no. 18, pp. 3611–3617, 2017.

[33] F. Zhang, W. N. Wang, H. P. Cong, L. B. Luo, Z. B. Zha, and H. S. Qian, "Facile synthesis of upconverting nanoparticles/zinc oxide core–shell nanostructures with large lattice mismatch for infrared triggered photocatalysis," *Particle & Particle Systems Characterization*, vol. 34, no. 2, article 1600222, 2017.

[34] F. Zhang, C. L. Zhang, H. Y. Peng, H. P. Cong, and H. S. Qian, "Near-infrared photocatalytic upconversion nanoparticles/TiO_2 nanofibers assembled in large scale by electrospinning," *Particle & Particle Systems Characterization*, vol. 33, no. 5, pp. 248–253, 2016.

[35] Y. Tang, W. di, X. Zhai, R. Yang, and W. Qin, "NIR-responsive photocatalytic activity and mechanism of $NaYF_4$:Yb,Tm@-TiO_2 core–shell nanoparticles," *ACS Catalysis*, vol. 3, no. 3, pp. 405–412, 2013.

[36] S. Zhuo, M. Shao, and S.-T. Lee, "Upconversion and downconversion fluorescent graphene quantum dots: ultrasonic preparation and photocatalysis," *ACS Nano*, vol. 6, no. 2, pp. 1059–1064, 2012.

[37] Y. Zhang and Z. Hong, "Synthesis of lanthanide-doped $NaYF_4$@TiO_2 core–shell composites with highly crystalline and tunable TiO_2 shells under mild conditions and their upconversion-based photocatalysis," *Nanoscale*, vol. 5, no. 19, pp. 8930–8933, 2013.

[38] Z. Zhang, W. Wang, W. Yin, M. Shang, L. Wang, and S. Sun, "Inducing photocatalysis by visible light beyond the absorption edge: effect of upconversion agent on the photocatalytic activity of Bi_2WO_6," *Applied Catalysis B: Environmental*, vol. 101, no. 1-2, pp. 68–73, 2010.

[39] Z. Zhang, W. Wang, J. Xu, M. Shang, J. Ren, and S. Sun, "Enhanced photocatalytic activity of Bi_2WO_6 doped with upconversion luminescence agent," *Catalysis Communications*, vol. 13, no. 1, pp. 31–34, 2011.

[40] R. Adhikari, G. Gyawali, S. H. Cho, R. Narro-Garcia, T. Sekino, and S. W. Lee, "Er^{3+}/Yb^{3+}co-doped bismuth molybdate nanosheets upconversion photocatalyst with enhanced photocatalytic activity," *Journal of Solid State Chemistry*, vol. 209, pp. 74–81, 2014.

[41] T. Zhou, J. Hu, and J. Li, "Er^{3+} doped bismuth molybdate nanosheets with exposed {0 1 0} facets and enhanced photocatalytic performance," *Applied Catalysis B: Environmental*, vol. 110, pp. 221–230, 2011.

[42] Y. Sun, W. Wang, S. Sun, and L. Zhang, "$NaYF_4$:Er,Yb/Bi_2MoO_6 core/shell nanocomposite: a highly efficient visible-light-driven photocatalyst utilizing upconversion," *Materials Research Bulletin*, vol. 52, pp. 50–55, 2014.

[43] J. Xu, R. Lv, S. du et al., "UCNPs@gelatin–ZnPc nanocomposite: synthesis, imaging and anticancer properties," *Journal of Materials Chemistry B*, vol. 4, no. 23, pp. 4138–4146, 2016.

[44] F. Zhang, C. L. Zhang, W. N. Wang, H. P. Cong, and H. S. Qian, "Titanium dioxide/upconversion nanoparticles/cadmium sulfide nanofibers enable enhanced full-spectrum absorption for superior solar light driven photocatalysis," *ChemSusChem*, vol. 9, no. 12, pp. 1449–1454, 2016.

[45] J. T. Xu, F. He, Z. Y. Cheng et al., "Yolk-structured upconversion nanoparticles with biodegradable silica shell for FRET sensing of drug release and imaging-guided chemotherapy," *Chemistry of Materials*, vol. 29, pp. 7615–7628, 2017.

[46] W. N. Wang, C. X. Huang, C. Y. Zhang et al., "Controlled synthesis of upconverting nanoparticles/$Zn_xCd_{1-x}S$ yolk-shell nanoparticles for efficient photocatalysis driven by NIR light," *Applied Catalysis B: Environmental*, vol. 224, pp. 854–862, 2018.

[47] W. Su, M. Zheng, L. Li et al., "Directly coat TiO_2 on hydrophobic $NaYF_4$:Yb,Tm nanoplates and regulate their photocatalytic

activities with the core size," *Journal of Materials Chemistry A*, vol. 2, no. 33, pp. 13486–13491, 2014.

[48] W. Wang, M. Ding, C. Lu, Y. Ni, and Z. Xu, "A study on upconversion UV–vis–NIR responsive photocatalytic activity and mechanisms of hexagonal phase $NaYF_4$:Yb^{3+},Tm^{3+}@TiO_2 core–shell structured photocatalyst," *Applied Catalysis B: Environmental*, vol. 144, pp. 379–385, 2014.

[49] X. Guo, C. Chen, D. Zhang, C. P. Tripp, S. Yin, and W. Qin, "Photocatalysis of $NaYF_4$:Yb,Er/CdSe composites under 1560 nm laser excitation," *RSC Advances*, vol. 6, no. 10, pp. 8127–8133, 2016.

[50] H. Fan, E. Leve, J. Gabaldon, A. Wright, R. E. Haddad, and C. J. Brinker, "Ordered two- and three-dimensional arrays self-assembled from water-soluble nanocrystal–micelles," *Advanced Materials*, vol. 17, no. 21, pp. 2587–2590, 2005.

[51] B. B. Ding, H. Y. Peng, H. S. Qian, L. Zheng, and S. H. Yu, "Unique upconversion core–shell nanoparticles with tunable fluorescence synthesized by a sequential growth process," *Advanced Materials Interfaces*, vol. 3, no. 3, 2016.

[52] J. Chen, B. B. Ding, T. Y. Wang et al., "Facile synthesis of uniform $Zn_xCd_{1-x}S$ alloyed hollow nanospheres for improved photocatalytic activities," *Journal of Materials Science: Materials in Electronics*, vol. 25, no. 9, pp. 4103–4109, 2014.

[53] J. Zhang, W.-N. Wang, M.-L. Zhao et al., "Magnetically recyclable Fe_3O_4@$Zn_xCd_{1-x}S$ core–shell microspheres for visible light-mediated photocatalysis," *Langmuir*, vol. 34, no. 31, pp. 9264–9271, 2018.

[54] H. Yoneyama, Y. Yamashita, and H. Tamura, "Heterogeneous photocatalytic reduction of dichromate on n-type semiconductor catalysts," *Nature*, vol. 282, no. 5741, pp. 817-818, 1979.

[55] S. E. Fendorf and R. J. Zasoski, "Chromium(III) oxidation by .delta.-manganese oxide (MnO2). 1. Characterization," *Environmental Science & Technology*, vol. 26, no. 1, pp. 79–85, 1992.

[56] Y. Nosaka and A. Y. Nosaka, "Generation and detection of reactive oxygen species in photocatalysis," *Chemical Reviews*, vol. 117, no. 17, pp. 11302–11336, 2017.

[57] H. Wang, S. Jiang, W. Shao et al., "Optically switchable photocatalysis in ultrathin black phosphorus nanosheets," *Journal of the American Chemical Society*, vol. 140, no. 9, pp. 3474–3480, 2018.